

Mesoscopic simulation of Brownian particles confined in harmonic traps and sheared fluids

J. Fernández and H. Híjar

*Grupo de Sistemas Inteligentes, Facultad de Ingeniería, Universidad La Salle,
Benjamín Franklin 47, 06140, D.F., México,*

e-mail: jaimefernandez@lasallistas.org.mx; humberto.hijar@lasallistas.org.mx

Received 13 August 2014; accepted 24 October 2014

We consider the motion of a Brownian particle bound by a harmonic force in a thermal bath driven from equilibrium by a uniform shear imposed externally. We extend the classical theory of Brownian motion to calculate the probability distribution function for finding the Brownian particle in a phase-space volume element when it is in the presence of the external shear. We find the explicit form of the reduced distribution for velocities in the stationary limit and show that it becomes anisotropic by extending itself over the direction of the imposed shear. We also consider the effects of the imposed shear on the time correlation functions of the Brownian particle and show that these quantities acquire contributions depending exclusively on the nonequilibrium state of the solvent, which render them non symmetric and time-irreversible. In order to verify these conclusions we develop a hybrid mesoscopic simulation technique based on Molecular Dynamics and Multi-particle Collision Dynamics. We observe a very good agreement between the predictions of the model and the results obtained independently from the simulation method, thus suggesting that the latter could be used as a complement to current experimental procedures.

Keywords: Brownian motion; nonequilibrium statistical mechanics; molecular dynamics; multi-particle collision dynamics.

PACS: 05.70.Ln; 05.40.Jc; 36.20.Ey

1. Introduction

The formulation of nonequilibrium thermodynamics for systems under shear represents a long standing problem that has received considerable attention during several decades [1, 2]. Special interest has been given to the case of Brownian motion in a shear flow, see *e.g.* Ref. 3 and references therein, since it represents one of the simplest models coupled to a nonequilibrium bath in which the effects of the external forces on the thermodynamic and transport properties can be investigated with significant detail. Diverse models ranging from kinetic theory [4, 5], Langevin and Fokker-Planck equations [6, 7], and Mesoscopic Nonequilibrium Thermodynamics [8–12], have been used to achieve this goal. In addition, Brownian motion in a shear flow has been proved to be amenable for experimental [13–16], and numerical [17–19] work.

The dynamics of a Brownian particle (BP) in a sheared fluid exhibits special features not observed in Brownian motion in an equilibrated thermal bath. In particular, shear modifies the motion of the BP by introducing non-thermal contributions in the diffusion tensor increasing with the magnitude of the velocity gradient of the imposed flow [3, 7]. It has been suggested that this dependence of diffusion on the external shear implies that the fundamental fluctuation-dissipation relation used in Langevin descriptions of Brownian motion is not longer valid out of equilibrium, but must be corrected to consider the effect of the external shear on the strength of the stochastic forces [7, 10]. In addition, the externally imposed flow breaks down the spatial symmetry and the time-reversibility of the dynamics of the BP [7]. This effect is exhibited by the behavior of the correlation functions of the

position and velocity vectors of the BP, which acquire asymmetric and time-irreversible contributions increasing with the magnitude of the shear rate [7].

In the present paper we will consider another relevant related model consisting of a BP in the presence of a simple shear flow and simultaneously bound by a harmonic force. Harmonic Brownian motion in flowing fluids was firstly considered several decades ago in Ref. 20. There, interest was focused in showing that harmonic constrains might lead to a sufficiently fast decay of the velocity correlation function of the BP to ensure the existence of a long-time diffusion behavior in external Couette and Poiseuille flows. Renewed interest for harmonically bound Brownian motion in external flows has been observed recently [21–23]. This interest has been greatly inspired by the development of experimental techniques based on optical tweezers which allow for manipulation of micro-sized particles, as well as for detailed measurement of their fluctuations. Theoretical analysis and experimental results confirm that harmonically bound Brownian motion in the presence of shear also exhibits the spatial asymmetry and time-irreversibility features predicted firstly for free Brownian motion in sheared fluids. More precisely, experiments with harmonically trapped BP's in a simple Couette flow have shown that cross correlation functions between displacements along the directions of shear and velocity gradient are indeed asymmetric and time-irreversible [21]. This result has been justified by a Langevin model [22], and has been also predicted to exist in the problem of controlling the trajectory of individual colloidal particles by means of optical traps in flowing fluids [23]. In the latter case, asymmetric, time-irreversible correlations have been observed by means of molecular simulations [23]. Although a similar nonequi-

librium behavior is expected for the velocity correlation functions, experimental techniques are not able to perform the corresponding measurements yet [21, 22]. The main contribution of the present work will consist in introducing a simulation technique from which it will be possible to verify the theoretical predictions about the behavior of the velocity correlation functions of a harmonically bound BP in a sheared fluid.

Our numerical implementation will consist of a hybrid algorithm combining Molecular Dynamics (MD) [24], which is used to describe the evolution of systems at the microscopic time scale; and Multi-particle Collision Dynamics (MPC) [25, 26], that allows for incorporating thermal fluctuations and hydrodynamic effects. Both MD and MPC are particle-based methods and their coupling has been used in simulations to incorporate a bridge that spans the two widely separated characteristic time scales occurring in Brownian motion, corresponding to the relaxation time of the solvent to thermodynamic equilibrium and to the time it takes to the BP to move a distance comparable with its own size. Numerical experiments combining MD and MPC have been successfully used to study concentrated nanocolloidal suspensions [26], colloid-fluid interactions [27], colloid sedimentation [28], backtracking of colloidal particles [29], colloidal flow in microfluidic channels [30], and tracking control of colloidal particles in fluids in stationary flow [23].

In Sec. 2 we will revisit the Langevin model for a harmonically bound BP in a sheared environment. We will carefully study the conditions under which the classical theory of Brownian motion can be indeed extended to this nonequilibrium situation. The formal solution of this model will be presented from which we will calculate the probability distribution function (PDF) for observing the BP in a given volume element of its phase-space. We will show that this distribution deviates by a significant amount from the canonical equilibrium distribution when the Brownian motion takes place in the presence of the velocity gradient. Subsequently, we will calculate the matrix of two-time correlation functions for the velocity components of the BP. These functions will be shown to be non symmetric and time-irreversible due to the external shear, in a similar fashion as it has been obtained for ordinary Brownian motion in a plane Couette flow. In Sec. 3 we will describe the implementation of the simulation method combining MD and MPC, designed to verify the predictions of the previously described model. In Sec. 4 we will present a comparison between the analytical and the numerical results. We will verify that the model based on Langevin dynamics and the implemented numerical method exhibit the same quantitative behavior, and that the latter can be effectively used to observe the breakdown of the spatial and temporal symmetry of the velocity correlation functions of a trapped BP under shear. Finally, in Sec. 5 we will summarize our conclusions and discuss the limitations of our analysis.

2. Harmonic Brownian Motion under Steady Shear

2.1. Langevin Dynamics

In the present section we will study the motion of a spherical BP of mass M and radius R , immersed in an incompressible Newtonian fluid which is in a nonequilibrium stationary state induced by a uniform shear. Specifically, we will consider the case in which the velocity field of the unperturbed fluid is a plane Couette flow of the form $\vec{v}(\vec{r}) = \vec{v}(0) + \mathbf{Z} \cdot \vec{r}$, where \vec{r} , $\vec{v}(0)$ and \mathbf{Z} represent, respectively, the position vector, the velocity at the origin and the constant velocity gradient tensor of the flow. Moreover, the flow will be assumed to be sheared along the \hat{e}_3 -axis with velocity increasing along the \hat{e}_1 direction, where vectors $\{\hat{e}_1, \hat{e}_2, \hat{e}_3\}$ represent the standard Cartesian basis. Thus, \mathbf{Z} will take the form

$$\mathbf{Z} = \begin{pmatrix} 0 & 0 & 0 \\ 0 & 0 & 0 \\ \dot{\gamma} & 0 & 0 \end{pmatrix}, \quad (1)$$

where $\dot{\gamma}$ is the magnitude of the velocity gradient.

We will consider the presence of an external force, \vec{F} , acting on the BP and use a Langevin model to describe its evolution in time, under the assumption that its dynamics occur at a time scale much larger than the corresponding to the fluctuations of the surrounding fluid. From now on, we will use the symbol \vec{A} to denote the stochastic force that models the random collisions of the BP with the molecules of the solvent. Finally, we will suppose that the friction term can be modeled by the Faxén theorem for the motion of a sphere through a viscous fluid in a non-homogeneous stationary flow [31, 32]. Therefore, the equation of motion of the BP will read

$$M \frac{d^2 \vec{x}}{dt^2} = -\gamma \frac{d\vec{x}}{dt} + \gamma \vec{v}^s(\vec{x}) + \vec{F} + \vec{A}, \quad (2)$$

where γ is the drag coefficient and $\vec{v}^s(\vec{x})$ represents the average of the unperturbed velocity field over the surface of the BP [32].

Let us assume now that the external force has the form

$$\vec{F} = -k(\vec{x} - \vec{r}_0), \quad (3)$$

where k is the restoring coefficient of an isotropic harmonic trap. This force is meant to constrain harmonically the motion of the BP around a fixed position in space, \vec{r}_0 , that without loss of generality is chosen in such a way that the velocity field \vec{v} vanishes there, *i.e.* $\vec{v}(\vec{r}_0) = 0$.

In addition, under the restriction of considering only Brownian motion in a plane Couette flow, we can write $\vec{v}^s(\vec{x})$ in terms of \mathbf{Z} , \vec{x} and \vec{r}_0 , namely $\vec{v}^s(\vec{x}) = \mathbf{Z} \cdot (\vec{x} - \vec{r}_0)$. By substituting $\vec{v}^s(\vec{x})$ and Eq. (3) into Eq. (2), we obtain

$$\frac{d^2 \vec{X}}{dt^2} + \beta \frac{d\vec{X}}{dt} + [\omega^2 \mathbf{1} - \beta \mathbf{Z}] \cdot \vec{X} = \vec{A}, \quad (4)$$

where we have written the result in terms of the position of the BP relative to the point \vec{r}_0 , $\vec{X} = \vec{x} - \vec{r}_0$; the damping

ratio $\beta = \gamma/M$; the frequency $\omega = \sqrt{k/M}$; the unit matrix, $\mathbf{1}$; and the stochastic force per unit mass $\vec{A} = \vec{A}/M$.

Then, it can be noticed that Eq. (4) is equivalent to a set of three stochastic damped oscillators asymmetrically coupled by the velocity gradient tensor \mathbf{Z} . Actually, since in the present model the position of the BP is controlled around \vec{r}_0 by a harmonic force, Eq. (4) turns out to be formally the same as the one obtained for the general problem of tracking control of colloidal particles in fluids in uniform shear, Eq. (23) in Ref. 23. In that reference attention was focused mainly in showing that harmonic forces can be properly tuned to oblige colloidal particles to follow any prescribed trajectory in spite of the presence of the external flow. Here, on the other hand, we will provide a full characterization of the stochastic dynamics of the trapped BP. For this purpose, we will use the formal solution of Eq. (4), obtained also in Ref. 23, and extend it to consider both the relative position vector, \vec{X} , and the velocity vector, $\vec{U} = d\vec{X}/dt$. It will prove to be convenient to write these functions in the form

$$\vec{X}(t) = \vec{X}_d(t) + \int_0^t d\xi \Psi(t-\xi) \cdot \vec{A}(\xi), \quad (5)$$

$$\vec{U}(t) = \vec{U}_d(t) + \int_0^t d\xi \Phi(t-\xi) \cdot \vec{A}(\xi), \quad (6)$$

where $\vec{X}_d(t)$ and $\vec{U}_d(t)$ represent the deterministic part of the solution of Eq. (4); and Ψ and Φ are auxiliary matrices to be defined below.

The components of \vec{X}_d were already presented by one of us in Eqs. (36)-(38) in Ref. 23.

The components of \vec{U}_d are obtained by derivation, *i.e.* by $\vec{U}_d = d\vec{X}_d/dt$, and explicitly read

$$U_{d,1}(t) = \frac{1}{\mu_1 - \mu_2} [\mu_2 (\mu_1 X_{0,1} - U_{0,1}) e^{\mu_2 t} - \mu_1 (\mu_2 X_{0,1} - U_{0,1}) e^{\mu_1 t}], \quad (7)$$

$$U_{d,2}(t) = \frac{1}{\mu_1 - \mu_2} [\mu_2 (\mu_1 X_{0,2} - U_{0,2}) e^{\mu_2 t} - \mu_1 (\mu_2 X_{0,2} - U_{0,2}) e^{\mu_1 t}], \quad (8)$$

and

$$U_{d,3}(t) = \frac{1}{\mu_1 - \mu_2} [\mu_2 (\mu_1 X_{0,3} - U_{0,3}) e^{\mu_2 t} - \mu_1 (\mu_2 X_{0,3} - U_{0,3}) e^{\mu_1 t}] + \frac{\dot{\gamma}\chi}{\mu_1 - \mu_2} \left\{ e^{\mu_1 t} \left[\left(1 + \mu_1 \left(t - \frac{2}{\mu_1 - \mu_2} \right) \right) (U_{0,1} - \mu_2 X_{0,1}) + \mu_1 X_{0,1} \right] + e^{\mu_2 t} \left[\left(1 + \mu_2 \left(t - \frac{2}{\mu_2 - \mu_1} \right) \right) (U_{0,1} - \mu_1 X_{0,1}) + \mu_2 X_{0,1} \right] \right\}. \quad (9)$$

In the previous expressions $X_{0,i}$ and $U_{0,i}$, for $i = 1, 2, 3$, represent the initial conditions; $\mu_{1,2} = -\beta/2 \pm ((\beta/2)^2 - \omega^2)^{1/2}$, are the roots of the characteristic polynomial of the homogeneous part associated to Eq. (4); and $\chi = (\mu_1 + \mu_2) / (\mu_2 - \mu_1)$ is a dimensionless parameter.

The matrix Ψ will be cast in the form

$$\Psi(t-\xi) = \begin{pmatrix} \psi(t-\xi) & 0 & 0 \\ 0 & \psi(t-\xi) & 0 \\ \dot{\gamma}\kappa(t-\xi) & 0 & \psi(t-\xi) \end{pmatrix}, \quad (10)$$

where the functions ψ and κ are defined through

$$\psi(t-\xi) = \frac{1}{\mu_1 - \mu_2} (e^{\mu_1(t-\xi)} - e^{\mu_2(t-\xi)}), \quad (11)$$

$$\kappa(t-\xi) = \chi \left[(t-\xi) \zeta(t-\xi) - \frac{2}{\mu_1 - \mu_2} \psi(t-\xi) \right], \quad (12)$$

with

$$\zeta(t-\xi) = \frac{1}{\mu_1 - \mu_2} (e^{\mu_1(t-\xi)} + e^{\mu_2(t-\xi)}); \quad (13)$$

and the matrix Φ can be obtained from $\Phi = d\Psi/dt$.

It should be mentioned here that it is in fact debatable to use a Langevin model like the one presented in this subsection for describing Brownian motion in fluids in nonequilibrium states. The main criticism that can be formulated against this procedure lays on the lack of a well established theory for describing the statistical properties of the stochastic forces produced by nonequibrated baths, while in the case in which the solvent is in equilibrium \vec{A} is very well modeled as a Markov-Gaussian process [33, 34].

For Brownian motion in sheared fluids, analytical models [10], experimental results [14] and numerical simulations [17] suggest that the fluctuating force is modified by the imposed velocity gradient \mathbf{Z} . However, it has been also discussed that nonequilibrium corrections to the strength of the stochastic forces are expected to be negligible since they have been shown to be of the order of the ratio of the fluid molecular relaxation time to the characteristic time of the imposed shear, *i.e.* to the ratio of a microscopic to a macroscopic quantity [5]. In the following we shall assume that the time scales of the white noise and the imposed flow are well separated and that, consequently, in the nonequilibrium situation \vec{A} is still a Markovian Gaussian stochastic vari-

able, with zero mean and obeying the classical (equilibrium) Fluctuation-Dissipation relation

$$\langle \vec{\mathcal{A}}(t') \vec{\mathcal{A}}(t) \rangle = \frac{2k_B T \beta}{M} \delta(t' - t) \mathbf{1}, \quad (14)$$

where the brackets, $\langle \langle \dots \rangle \rangle$, indicate the average over fluctuations and initial conditions; k_B is the Boltzmann constant; T is the temperature of the bath; and $\delta(t' - t)$ is the Dirac delta function.

2.2. Nonequilibrium Probability Distribution Function

Equations (7)-(13) clearly illustrate that the nonequilibrium coupling induced by the velocity gradient in the motion of the harmonically bound BP is asymmetric since the components along the shear are perturbed by the stochastic forces and initial conditions in the direction of the velocity gradient, but the converse fact is not true. The effects of this asymmetry produced by the external shear will be analyzed by generalizing the classical theory of Brownian motion as presented *e.g.* in Refs. 33 and 35, to the present nonequilibrium case.

With this purpose let us define firstly the auxiliary vectors $\vec{R}(t) = \vec{X}(t) - \vec{X}_d(t)$, and $\vec{S}(t) = \vec{U}(t) - \vec{U}_d(t)$. Their probability distribution can be calculated by using the assumption that the stochastic forces $\vec{\mathcal{A}}$ vary in time extremely rapidly when compared with the variables representing the state of the BP. In this case, the integrals appearing in Eqs. (5) and (6) can be written as sums of \tilde{N} integrals over equal time intervals of size $\delta t = t/\tilde{N}$, such that δt is large with respect to the characteristic time of relaxation of fluctuations but small in comparison with the time scale for changes in \vec{R} and \vec{S} . This procedure yields

$$\vec{R}(t) = \sum_{j=1}^{\tilde{N}} \Psi(t - j\delta t) \cdot \vec{B}_j(\delta t), \quad (15)$$

and

$$\vec{S}(t) = \sum_{j=1}^{\tilde{N}} \Phi(t - j\delta t) \cdot \vec{B}_j(\delta t), \quad (16)$$

where \vec{B}_j is the net stochastic acceleration suffered by the BP in the j th time interval, *i.e.*

$$\vec{B}_j(\delta t) = \int_{j\delta t}^{(j+1)\delta t} d\xi \vec{\mathcal{A}}(\xi). \quad (17)$$

The probability $W(\vec{R}, \vec{S}; t) d\vec{R} d\vec{S}$ that vectors \vec{R} and \vec{S} will be found in the intervals $(\vec{R}, \vec{R} + d\vec{R})$ and $(\vec{S}, \vec{S} + d\vec{S})$, respectively, at time t after \tilde{N} accelerations, can be obtained analogously to the case of the general problem of random flights [33], under the assumption that \vec{B} follows a Markov process. Thus we obtain

$$W(\vec{R}, \vec{S}; t) d\vec{R} d\vec{S} = d\vec{R} d\vec{S} \frac{1}{(2\pi)^6} \int d\vec{\rho} \times \int d\vec{\sigma} e^{-i(\vec{\rho}^T \cdot \vec{R} + \vec{\sigma}^T \cdot \vec{S})} \Omega_{\tilde{N}}(\vec{\rho}, \vec{\sigma}), \quad (18)$$

where $\vec{\rho}$ and $\vec{\sigma}$ are auxiliary vectors, the superscript T denotes the transpose of the corresponding vector or matrix, and the function $\Omega_{\tilde{N}}(\vec{\rho}, \vec{\sigma})$ is defined by

$$\Omega_{\tilde{N}}(\vec{\rho}, \vec{\sigma}) = \prod_{j=1}^{\tilde{N}} \int d\vec{B}_j w(\vec{B}_j) \times e^{i[\vec{\rho}^T \cdot \Psi(t-j\Delta t) \cdot \vec{B}_j + \vec{\sigma}^T \cdot \Phi(t-j\Delta t) \cdot \vec{B}_j]}, \quad (19)$$

with $w(\vec{B}_j) d\vec{B}_j$ the probability of observing an acceleration \vec{B}_j in the interval $(\vec{B}_j, \vec{B}_j + d\vec{B}_j)$.

As it was previously mentioned, one of the main assumptions to be introduced in the present analysis will consist in considering that the probability of occurrence of different values of the stochastic force, and consequently of \vec{B}_j , is independent of the imposed external shear, *i.e.* it is the same than in the equilibrium case. Thus, we have [33]

$$w(\vec{B}_j) d\vec{B}_j = \frac{1}{(4\pi q \delta t)^{3/2}} e^{(-\vec{B}_j \cdot \vec{B}_j / 4q \delta t)} \quad (20)$$

with $q = \beta k_B T / M$. By replacing Eq. (20) into Eq. (19), and calculating the resulting Gaussian integrals in the limit $\delta t \rightarrow 0$, we obtain the following expression for the auxiliary function $\Omega_{\tilde{N}}$,

$$\Omega_{\tilde{N}}(\vec{\rho}, \vec{\sigma}) = \exp \left[-\frac{1}{2} (\vec{\rho}^T \cdot \mathbf{P} \cdot \vec{\rho} + \vec{\rho}^T \cdot \mathbf{R} \cdot \vec{\sigma} + \vec{\sigma}^T \cdot \mathbf{R}^T \cdot \vec{\rho} + \vec{\sigma}^T \cdot \mathbf{Q} \cdot \vec{\sigma}) \right], \quad (21)$$

where the matrices $\mathbf{P} = \mathbf{P}(t)$, $\mathbf{Q} = \mathbf{Q}(t)$ and $\mathbf{R} = \mathbf{R}(t)$ have, respectively, the form

$$\mathbf{P}(t) = 2q \int_0^t d\xi \begin{pmatrix} \psi^2(\xi) & 0 & \dot{\gamma} \psi(\xi) \kappa(\xi) \\ 0 & \psi^2(\xi) & 0 \\ \dot{\gamma} \psi(\xi) \kappa(\xi) & 0 & \psi^2(\xi) + \dot{\gamma}^2 \kappa^2(\xi) \end{pmatrix}, \quad (22)$$

$$\mathbf{Q}(t) = 2q \int_0^t d\xi \begin{pmatrix} \phi^2(\xi) & 0 & \dot{\gamma} \phi(\xi) \lambda(\xi) \\ 0 & \phi^2(\xi) & 0 \\ \dot{\gamma} \phi(\xi) \lambda(\xi) & 0 & \phi^2(\xi) + \dot{\gamma}^2 \lambda^2(\xi) \end{pmatrix}, \quad (23)$$

$$\mathbf{R}(t) = 2q \int_0^t d\xi \begin{pmatrix} \psi(\xi) \phi(\xi) & 0 & \dot{\gamma} \psi(\xi) \lambda(\xi) \\ 0 & \psi(\xi) \phi(\xi) & 0 \\ \dot{\gamma} \phi(\xi) \kappa(\xi) & 0 & \psi(\xi) \phi(\xi) + \dot{\gamma}^2 \kappa(\xi) \lambda(\xi) \end{pmatrix}. \quad (24)$$

In the last two equations functions ϕ and λ , have been defined as $\phi = d\psi/dt$ and $\lambda = d\kappa/dt$, respectively.

Finally, by replacing Eq. (21) into Eq. (18), and calculating the integral over the space of the auxiliary vectors $\vec{\rho}$ and $\vec{\sigma}$, we arrive at

$$W(\vec{R}, \vec{S}; t) d\vec{R} d\vec{S} = \frac{\exp\left\{-\frac{1}{2}(\vec{R}^T, \vec{S}^T) \cdot \mathbf{H}^{-1}(t) \cdot \begin{pmatrix} \vec{R} \\ \vec{S} \end{pmatrix}\right\}}{(2\pi)^3 (\det \mathbf{H}(t))^{1/2}} d\vec{R} d\vec{S}, \quad (25)$$

where $\mathbf{H}(t)$ is a 6×6 symmetric matrix defined by the partition

$$\mathbf{H}(t) = \begin{pmatrix} \mathbf{P}(t) & \mathbf{R}(t) \\ \mathbf{R}^T(t) & \mathbf{Q}(t) \end{pmatrix}. \quad (26)$$

As it is usual, in the previous expression $\mathbf{H}^{-1}(t)$ and $\det \mathbf{H}(t)$ denote the inverse and determinant of $\mathbf{H}(t)$, respectively.

Equations (22)-(26) contain all the effects produced by the nonequilibrium bath on the statistical properties of the harmonically bound BP. They show that the PDF for this particle is a Gaussian, as in the equilibrium case, but anisotropic due to the presence of the external shear. The effects of the imposed flow on the distribution W can be analyzed by considering the explicit form acquired by this function in the important limit of large times, $t \gg \beta^{-1}$, where W becomes stationary. In particular, by considering the stationary limit of the matrices \mathbf{P} , \mathbf{R} and \mathbf{Q} , and integrating over the coordinates $\{X_1, X_2, X_3, U_2\}$, we obtain the reduced probability of observing the velocities U_1 and U_3 in the ranges $(U_1, U_1 + dU_1)$ and $(U_3, U_3 + dU_3)$, respectively, which explicitly reads

$$W(U_1, U_3) dU_1 dU_3 = \frac{M}{2\pi k_B T \sqrt{1 + \dot{\gamma}^2/2\omega^2}} \times \exp\left\{-\frac{M}{2k_B T} \left[U_1^2 + \frac{U_3^2}{1 + \dot{\gamma}^2/2\omega^2}\right]\right\} dU_1 dU_3. \quad (27)$$

This result shows that the net effect of the external shear on the distribution of velocities of the BP consists in extending it along the direction of the imposed flow, while in the direction of the velocity gradient the distribution is not modified and remains the Maxwell function of equilibrium.

2.3. Correlation Functions

The effects of the velocity gradient of the solvent on the dynamics of the BP can be also analyzed in terms of the two-time correlation functions of the variables \vec{X} and \vec{U} . Since no numerical neither experimental measurements of correlation functions of the type $\langle\langle U_i(t') U_j(t) \rangle\rangle$ have been reported in the literature, our interest will be focused in the calculation of these quantities, where double brackets will be used to indicate the average over both fluctuations and initial conditions. It can be readily seen from Eqs. (6)-(9) that the desired correlations will have the general form

$$\langle\langle U_i(t') U_j(t) \rangle\rangle = \langle\langle U_i(t') U_j(t) \rangle\rangle^{\text{eq}} + \langle\langle U_i(t') U_j(t) \rangle\rangle^{\text{neq}}, \quad (28)$$

where the superscripts eq and neq represent, respectively, those contributions independent of the external velocity gradient, and those induced exclusively by the nonequilibrium state of the solvent and explicitly depending on $\dot{\gamma}$.

The correlation functions defined in the previous equation will be calculated over an ensemble of BPs that have been allowed to evolve in the nonequilibrium thermal bath for a sufficient long time in such a way that the initial conditions $X_{0,i}$ and $U_{0,i}$ appearing in Eqs. (7)-(9) can be assumed to be sampled from the nonequilibrium PDF in the asymptotic limit. Thus, in calculating the correlation functions the elements of the following dyad matrix containing the averages of products of initial coordinates will be used

$$\begin{pmatrix} \langle\langle \vec{X}_0 \vec{X}_0 \rangle\rangle & \langle\langle \vec{X}_0 \vec{U}_0 \rangle\rangle \\ \langle\langle \vec{U}_0 \vec{X}_0 \rangle\rangle & \langle\langle \vec{U}_0 \vec{U}_0 \rangle\rangle \end{pmatrix} = \int d\vec{X} \int d\vec{U} W(\vec{X}, \vec{U}) \begin{pmatrix} \vec{X} \vec{X} & \vec{X} \vec{U} \\ \vec{U} \vec{X} & \vec{U} \vec{U} \end{pmatrix} \\ = \frac{k_B T}{k} \begin{pmatrix} 1 & 0 & \frac{\dot{\gamma} \beta}{2\omega^2} & 0 & 0 & \frac{\dot{\gamma}}{2} \\ 0 & 1 & 0 & 0 & 0 & 0 \\ \frac{\dot{\gamma} \beta}{2\omega^2} & 0 & \left[1 + \dot{\gamma}^2 \frac{\omega^2 + \beta^2}{2\omega^4}\right] & -\frac{\dot{\gamma}}{2} & 0 & 0 \\ 0 & 0 & -\frac{\dot{\gamma}}{2} & \omega^2 & 0 & 0 \\ 0 & 0 & 0 & 0 & \omega^2 & 0 \\ \frac{\dot{\gamma}}{2} & 0 & 0 & 0 & 0 & \omega^2 \left(1 + \frac{\dot{\gamma}^2}{\omega^2}\right) \end{pmatrix}. \quad (29)$$

A direct but rather long algebraic procedure consisting in evaluating the formal solution of the Langevin equation, Eqs. (6)-(9), at two different times t' and t , with $t' > t$, multiplying the results and calculating the average over the initial conditions and stochastic forces, with the help of Eqs. (14) and (29), yields the expressions presented below for the elements of the correlation matrix.

As they should, the equilibrium contributions are stationary, *i.e.* they depend only on the time difference $\tau = t' - t$, and have the classical form [33]

$$\langle\langle U_i(t') U_j(t) \rangle\rangle^{\text{eq}} = \frac{k_B T}{M(\mu_1 - \mu_2)} [\mu_1 e^{\mu_1 \tau} - \mu_2 e^{\mu_2 \tau}] \delta_{ij}. \quad (30)$$

On the other hand, it can be noticed from Eqs. (7)-(9) that the only non vanishing nonequilibrium elements of the correlation matrix are $\langle\langle U_1(t') U_3(t) \rangle\rangle^{\text{neq}}$, $\langle\langle U_3(t') U_1(t) \rangle\rangle^{\text{neq}}$ and $\langle\langle U_3(t') U_3(t) \rangle\rangle^{\text{neq}}$. They are found to be stationary as the equilibrium contributions, and to have the following explicit form

$$\langle\langle U_1(t') U_3(t) \rangle\rangle^{\text{neq}} = -\frac{k_B T}{2M(\mu_1 - \mu_2)} \dot{\gamma} (e^{\mu_1 \tau} - e^{\mu_2 \tau}), \quad (31)$$

$$\begin{aligned} \langle\langle U_3(t') U_1(t) \rangle\rangle^{\text{neq}} &= \frac{k_B T}{2M(\mu_1 - \mu_2)} \dot{\gamma} \left\{ \left[1 + 2 \left(\frac{\mu_1 + \mu_2}{\mu_1 - \mu_2} \right)^2 - 2\mu_1 \tau \frac{\mu_1 + \mu_2}{\mu_1 - \mu_2} \right] e^{\mu_1 \tau} \right. \\ &\quad \left. - \left[1 + 2 \left(\frac{\mu_1 + \mu_2}{\mu_1 - \mu_2} \right)^2 - 2\mu_2 \tau \frac{\mu_1 + \mu_2}{\mu_2 - \mu_1} \right] e^{\mu_2 \tau} \right\}, \end{aligned} \quad (32)$$

and

$$\begin{aligned} \langle\langle U_3(t') U_3(t) \rangle\rangle^{\text{neq}} &= \frac{k_B T}{M} \frac{\dot{\gamma}^2}{2(\mu_1 - \mu_2)^3} \left[-\frac{\mu_1^2 (3 - \mu_1 \tau) + \mu_2^2 (1 + \mu_1 \tau)}{\mu_1} e^{\mu_1 \tau} \right. \\ &\quad \left. + \frac{\mu_2^2 (3 - \mu_2 \tau) + \mu_1^2 (1 + \mu_2 \tau)}{\mu_2} e^{\mu_2 \tau} \right], \end{aligned} \quad (33)$$

respectively.

Equations (31)-(33) summarize some of the main conclusions of the present work. They show that $\dot{\gamma}$ breaks the spatial symmetry of the dynamics of the Brownian oscillator by inducing a clear difference in its correlation functions in the directions of shear, \hat{e}_3 , and of increasing velocity, \hat{e}_1 . Accordingly, the autocorrelation function in the shear direction becomes higher than the corresponding correlation in the direction of the velocity gradient by the term proportional to $\dot{\gamma}^2$ given by Eq. (33). More strikingly, cross-correlations along these directions, which vanish in Brownian motion in a fluid at rest, become visible in the nonequilibrium case and one another exhibit a completely different time dependence, namely while $\langle\langle U_1(t') U_3(t) \rangle\rangle^{\text{neq}}$ decreases initially from zero as function of τ , $\langle\langle U_3(t') U_1(t) \rangle\rangle^{\text{neq}}$ increases, and both correlations eventually decay asymptotically. Furthermore, it can be observed from Eqs. (31) and (32) that cross correlations are time-irreversible, *i.e.* that $\langle\langle U_1(t + \tau) U_3(t) \rangle\rangle^{\text{neq}} \neq \langle\langle U_3(t + \tau) U_1(t) \rangle\rangle^{\text{neq}}$, and consequently, $\dot{\gamma}$ is found to break also the time-reversibility in the dynamics of the harmonic BP. These features will be further analyzed in Sec. 4., where we will show that the nonequilibrium induced effects can be significant, *i.e.* of the same order of magnitude of the equilibrium correlations, and can be actually seen in numerical experiments.

The behavior of the nonequilibrium correlations described in the preceding paragraph is similar to the one derived in previous models for correlations of free BPs moving in a plane Couette flow [7], and guided by harmonic traps in a sheared fluid [23]. However, one fundamental difference can be observed to exist between our results and those reported previously, namely, that our nonequilibrium correlation functions are stationary while they have been claimed to be non stationary in the previous references. The source of this discrepancy is that in Refs. 7 and 23 initial conditions have been assumed to be sampled from the canonical equilibrium distribution, while here we have used the proper nonequilibrium PDF in the asymptotic limit to perform the average over initial conditions, Eq. (29). By following this procedure we observe that all the non stationary contributions to the correlation functions cancel each other exactly and vanish.

Finally, in order to conclude the present section we would like to notice that the diagonal elements of the matrix in Eq. (29), are directly related with the average potential and kinetic energies of the harmonically bound BP. Consequently, Eq. (29) indicates that one additional effect of the imposed flow on the dynamics of the trapped BP consists in modifying its total energy, an effect that can be described in terms of an

effective nonequilibrium temperature increasing as $\dot{\gamma}^2$ [36], and showing that the net effect of the external shear flow is to increase the strength of the random thermal motion of the harmonic BP.

3. Simulation Method

3.1. Hybrid MD-MPC Algorithm

We performed numerical experiments in order to observe the effects produced by the externally imposed shear on the dynamics of the harmonically bound BP. As it was previously mentioned in Sec. 1, our implementation consisted of a hybrid technique combining MD and MPC. We considered N fluid particles of mass m , and a single BP of mass M , moving in a cubic simulation box of volume L^3 . Solvent particles were assumed to be point particles and in order to achieve their coupling with the BP an explicit interaction force was introduced. This force was derived from the Weeks-Chandler-Andersen (WCA) potential [37]

$$\Phi = \begin{cases} 4\epsilon \left[\left(\frac{\sigma}{|\vec{x}_i - \vec{x}|} \right)^{12} - \left(\frac{\sigma}{|\vec{x}_i - \vec{x}|} \right)^6 + \frac{1}{4} \right], & \text{if } |\vec{x}_i - \vec{x}| \leq 2\frac{1}{6}\sigma \\ 0, & \text{otherwise} \end{cases} \quad (34)$$

where ϵ is the interaction strength, σ the effective diameter of the interaction, and \vec{x}_i and \vec{x} the position vectors of the i th fluid particle and the BP, respectively.

In hybrid MD-MPC simulations the system evolves in time in a succession of propagation and collision steps. While propagation steps are carried out at short time intervals of size Δt_{MD} , collision steps take place only at regular, larger periods of time of size $\Delta t > \Delta t_{\text{MD}}$. In a propagation step, the positions and velocities of all the particles in the system are updated by integrating the Newton's equations of motion through a MD scheme over the time-step Δt_{MD} . In our simulations we achieved the coupling between MD and MPC by applying the velocity-Verlet propagation algorithm [24]. Accordingly, for fluid particles we used the rules [24]

$$\begin{aligned} \vec{x}_i(t + \Delta t_{\text{MD}}) &= \vec{x}_i(t) \\ &+ \Delta t_{\text{MD}} \vec{u}_i(t) + \frac{(\Delta t_{\text{MD}})^2}{2m} \vec{f}_i(t), \end{aligned} \quad (35)$$

and

$$\begin{aligned} \vec{u}_i(t + \Delta t_{\text{MD}}) &= \vec{u}_i(t) \\ &+ \frac{\Delta t_{\text{MD}}}{2m} \left[\vec{f}_i(t + \Delta t_{\text{MD}}) + \vec{f}_i(t) \right], \end{aligned} \quad (36)$$

where $i = 1, 2, \dots, N$; \vec{u}_i is the velocity of the i -th particle and \vec{f}_i is the total force exerted on it, produced only by the WCA potential given by Eq. (34).

Analogously, the position and velocity vectors of the BP were integrated by

$$\vec{x}(t + \Delta t_{\text{MD}}) = \vec{x}(t) + \Delta t_{\text{MD}} \vec{u}(t) + \frac{(\Delta t_{\text{MD}})^2}{2M} \vec{f}(t), \quad (37)$$

and

$$\begin{aligned} \vec{u}(t + \Delta t_{\text{MD}}) &= \vec{u}(t) \\ &+ \frac{\Delta t_{\text{MD}}}{2M} \left[\vec{f}(t + \Delta t_{\text{MD}}) + \vec{f}(t) \right], \end{aligned} \quad (38)$$

respectively, where \vec{f} is the total force acting on the BP, *i.e.* the sum of the contribution arising from its interaction with the solvent particles, as stated by Eq. (34), and the external harmonic force \vec{F} .

The dynamics of the solvent was simulated in a coarse-grained manner by avoiding the use of direct interactions between particles of the fluid but incorporating the characteristic collision step of MPC. Specifically, we implemented the original collision rule for MPC, known as Stochastic Rotation Dynamics (SRD) [27, 38, 39]. Accordingly, at the regular periods of time of size Δt , the simulation box was subdivided into smaller cells of volume a^3 . The observed number of particles varied from cell to cell, although the average number of particles per cell, n_0 , was fixed throughout the simulation. The center of mass velocity was then calculated for every cell and the particles located within the same cell were forced to perform a fictitious collision by changing their velocities according to

$$\vec{u}'_i(t) = \vec{u}_{\text{cm}}(t) + \mathbf{R}(\alpha; \hat{e}(t)) \cdot [\vec{u}_i(t) - \vec{u}_{\text{cm}}(t)]. \quad (39)$$

In the previous expression \vec{u}_{cm} represents the center of mass velocity of the cell where the i th particle is located and $\mathbf{R}(\alpha; \hat{e}(t))$ is a stochastic rotation matrix. Indeed, \mathbf{R} rotates the velocities by a fixed angle α around the axis \hat{e} , which was chosen at random for each collision cell by selecting a point on the surface of a sphere from a uniform probability distribution.

We applied a homogeneous displacement of the MPC cells by a vector with random components uniformly distributed in between $-a/2$ and $a/2$, before the collision took place, in order to guarantee the Galilean invariance of the method as it was noticed firstly by Ihle and Kroll [40, 41].

In Fig. 1 we present a schematic illustration of the simulated system, where the three Cartesian directions are shown. For this reference frame we used periodic boundary conditions along the x_2 and x_3 directions, and Lees-Edwards boundary conditions (LEBC) [42] along the x_1 -direction in order to drive the system to a nonequilibrium state characterized by a stable linear velocity profile. Thus, if a particle was observed to leave the simulation box at the point $(-L/2, x_{i,2}, x_{i,3})$, it was replaced by a particle with coordinates $(L/2, x_{i,2}, x_{i,3} + \dot{\gamma}L/2)$ and velocity $(u_{i,1}, u_{i,2}, u_{i,3} + \dot{\gamma}L/2)$; while every particle that moved out of the box at $(L/2, x_{i,2}, x_{i,3})$ was substituted by another particle at $(-L/2, x_{i,2}, x_{i,3} - \dot{\gamma}L/2)$ with velocity $(u_{i,1}, u_{i,2}, u_{i,3} - \dot{\gamma}L/2)$. The application of these boundary driven conditions allowed for simulating a planar Couette flow in the system of the form $\vec{v}(\vec{r}) = \vec{v}(0) + \mathbf{Z} \cdot \vec{r}$, with \mathbf{Z} given by Eq. (1) and $\vec{v}(0) = -\dot{\gamma}L/2$. This velocity profile is also shown schematically in Fig. 1.

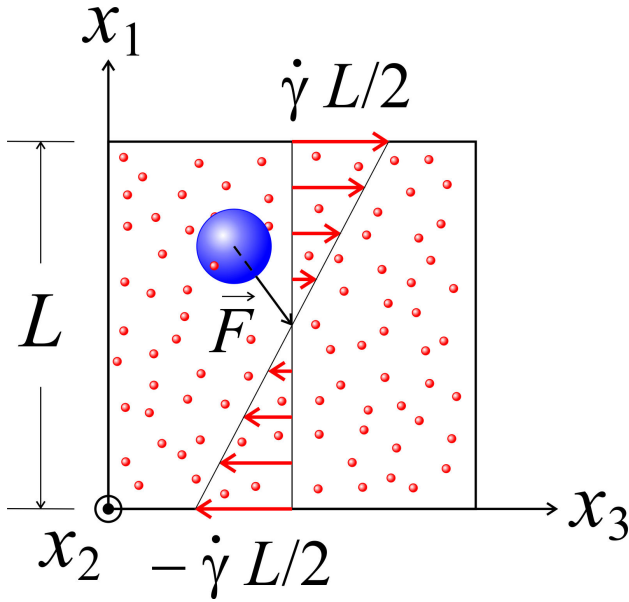


FIGURE 1. (Color online) Schematic illustration of the simulated system. The BP is represented by a big blue sphere, while solvent particles are represented by small red spheres. The application of LEBC, as it is described in the text, establishes the planar Couette flow represented by the red arrows. The harmonic force on the BP, \vec{F} , is directed towards the center of the simulation box.

It should be remarked that viscous heating is generated in MPC fluids when a plane Couette flow is established by the application of LEBC, and it is necessary to apply a thermostating procedure to prevent this effect and to achieve a true thermodynamic stationary state [28, 43–45]. Diverse thermostating procedures exist in literature which can be used to keep the temperature of MPC systems fluctuating around an average value [38]. The effects of these thermostats on the thermodynamic and transport properties of MPC fluids have been discussed recently [38, 46, 47]. Here we incorporated into our algorithm one of the simplest thermostating implementations in which the temperature is fixed at the local level by rescaling the velocities of the particles located within the same cell. Thus, velocities were changed after each collision step according to

$$\vec{u}'_i(t) = \vec{u}_{\text{cm}}(t) + \frac{T'(t)}{T} [\vec{u}_i(t) - \vec{u}_{\text{cm}}(t)]. \quad (40)$$

In Eq. (40), T is the fixed temperature of the thermostat and $T'(t)$ is the current temperature of the cell, *i.e.*

$$T'(t) = \frac{1}{3[n(t) - 1]k_B} \sum_{j=1}^{n(t)} m_j [\vec{u}_j(t) - \vec{u}_{\text{cm}}(t)]^2, \quad (41)$$

where the summation extends over the particles contained in the cell at time t , $n(t)$.

It can be noticed that due to the application of the external harmonic force there exists a momentum transfer from the BP to the solvent. Although this amount of transferred momentum would be expected to average zero for long-lasting simulations and to be negligible for sufficiently large systems, for

short-time simulations and finite systems it might induce a net flow of the solvent that will eventually perturb the dynamics of the BP. In a first approach we decided to implement a momentum reset step with the purpose of reducing this effect. This situation is similar to the one discussed in Refs. 23 and 43 where procedures for sustaining a zero net momentum in MPC simulations supplemented with LEBC have been introduced. Once again, we chose the simplest scheme in which a uniform velocity shift of the solvent particles was produced according to

$$\vec{u}'_i(t) = \vec{u}_i(t) + \frac{\vec{p}'(t) - \vec{p}}{mN}, \quad (42)$$

where $\vec{p}'(t)$ and \vec{p} are the total momentum of the solvent at time t and at the beginning of the simulation, respectively. This velocity shift was incorporated after the application of the thermostating step.

We performed our simulations according to the following general schedule. Initially, particles were placed in the simulation box at random positions and with random velocities obtained from uniform distributions. Overlapping between the fluid particles and the BP was avoided, the total momentum of the system was fixed to zero, and its total energy was fixed to the value of the equipartition law at the temperature of the thermostat. Then, the hybrid MD-MPC algorithm was applied over a sufficiently large time period in order to guarantee that the proper distribution of velocities and hydrodynamic fields were established. At this thermalization stage there was no restoring force acting on the BP. Finally, this force was applied according to Eq. (3) with \vec{r}_0 fixed at the center of the simulation box, as it is schematically shown in Fig. 1. The position and velocity vectors of the BP were stored as functions of the simulation time in order to calculate subsequently their statistical properties.

The specific implemented numerical setups and the results obtained from them will be presented in the subsequent sections, where we will use simulation units rather than physical units.

3.2. Simulation Parameters

In the present work we decided to use the quantities m , T , a , Δt , α , and n_0 as the independent parameters of the MPC method [25, 39]. Specifically, they were chosen to be, in simulation units, $m = 1$, $k_B T = 1$, $a = 1$, $\alpha = 135^\circ$, $\Delta t = 0.1$ and $n_0 = 3$. These values were selected with the purpose of tuning the properties of the MPC fluid in a regime where collisional effects dominate over propagation or kinematic effects. More precisely, for these parameters the collisional dynamics contributes to the kinematic viscosity of the MPC fluid with a term $\nu_{\text{col}} = 0.648$, while the contribution of the propagation dynamics is only $\nu_{\text{kin}} = 0.085$, as it can be verified from the analytical expressions obtained for these quantities in the SRD scheme in Refs. 40, 41, 48 and 49. On the other hand, MD parameters were fixed at $\epsilon = 2.5 k_B T$,

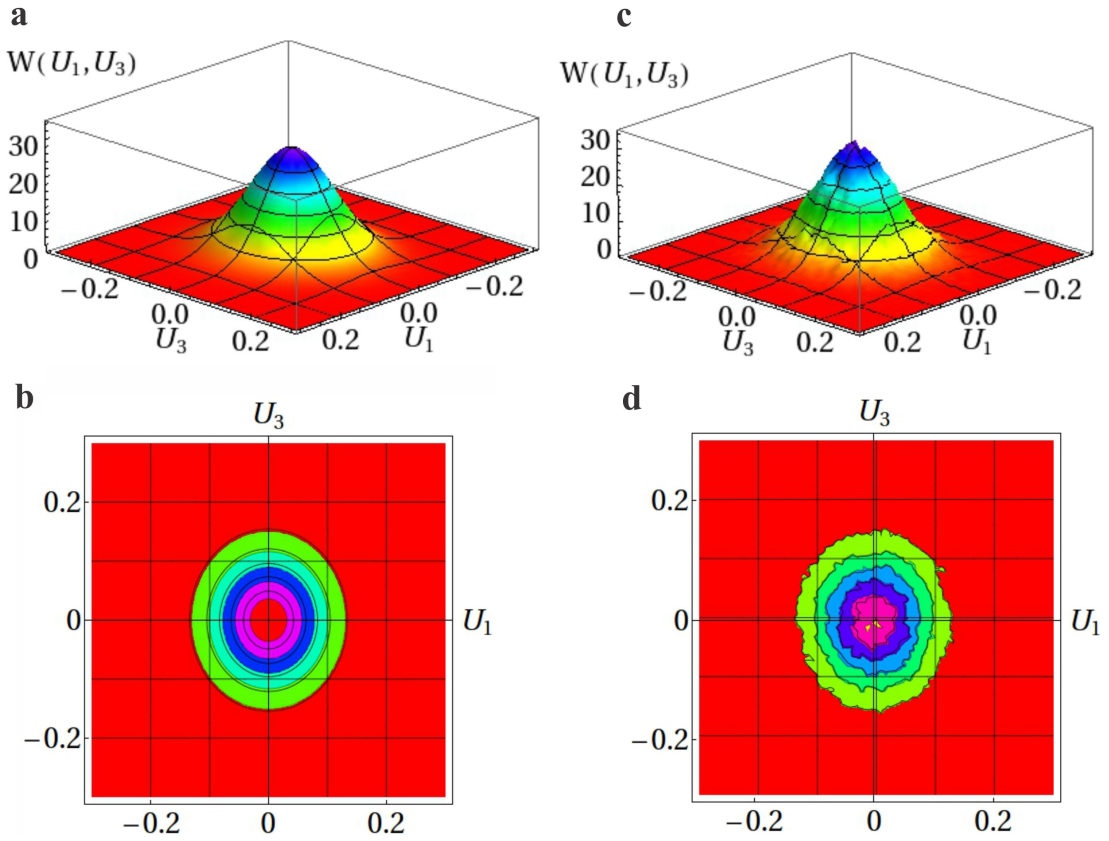


FIGURE 2. (Color online) Probability distribution function for the velocities U_1 and U_3 of the harmonically bound BP coupled to a nonequilibrium fluid with velocity gradient $\dot{\gamma} = 0.1$, in the case of critically damped dynamics. Cases **a** and **b** were obtained analytically from Eq. (27), while cases **c** and **d** were obtained independently from the simulation method combining MD and MPC described in Sec. 3.

$\sigma = 2a$, $\Delta t_{\text{MD}} = \Delta t/200$, and $M = 200m$. Finally, the size of the simulation box was fixed at $L = 20a$.

It should be remarked that this selection of parameters is identical to one used in Ref. 23 for the simulation of tracking control of colloidal particles. There it was discussed that no instabilities are expected for the MD algorithm and that the Brownian dynamics is expected to behave close to the Markovian description [27]. Moreover, the effective friction coefficient for the BP was also calculated for this numerical setup and it was found to be within the range $\gamma = 48.9 \pm 1.6$.

We kept the previous parameters fixed and considered two implementations in which the force constant, k , took values selected to reproduce the dynamics of the bound BP in the critically damped and under damped regimes. Respectively, these values were $k = 2.9928 \simeq \gamma^2/4M$ and $k = 4.0$.

4. Results

We shall present now the results obtained from the numerical method described in Sec. 3. and compare them with the analytical predictions of the model based on Langevin dynamics introduced in Sec. 2.. We will present our results in two subsections, the first one describing the comparison between the analytical and numerical nonequilibrium distribution functions, and the second one describing the behavior of the correlation functions of the harmonically bound BP.

4.1. Nonequilibrium Probability Distribution Functions

We performed numerical experiments for harmonic Brownian motion in fluids under plane Couette flows with five different values of the velocity gradient. In numerical units these values were chosen to be $\dot{\gamma} = 0$ (equilibrium), 0.01, 0.025, 0.05 and 0.1. Notice that for these values of $\dot{\gamma}$, the Stokes number $\mathcal{S} = \dot{\gamma}/\beta$, characterizing the deviation from equilibrium in terms of the BP's dynamics [7, 23], takes a maximum value of $\mathcal{S} = 0.4$, which is one order of magnitude smaller than those considered in the study of Brownian motion in shear flow in the absence of harmonic constraints [7]. However, we will show that the nonequilibrium effects of the external flow can be significant even for such small values of \mathcal{S} .

As it was mentioned before, we carried out the simulations for nonequilibrium stochastic harmonic oscillators in the regimes of critically-damped ($k = 2.9928$) and under damped ($k = 4.0$) dynamics. Thus, we performed a total of ten simulation experiments. Due to limitations in the computational resources available for the present research, our simulations were executed by allowing systems to thermalize in 2×10^6 steps of the MD-MPC algorithm, and extending further over 5×10^7 steps used to generate a time series were the values taken by \vec{U} at regular time intervals of size $25\Delta t_{\text{MD}}$

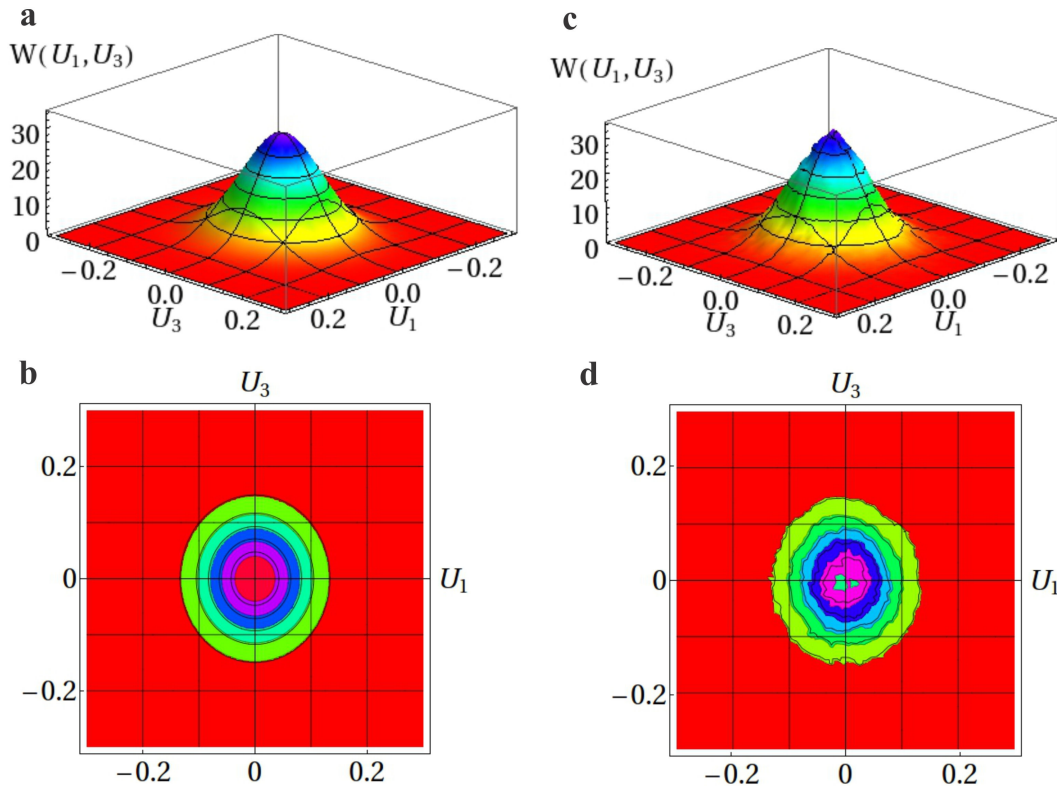


FIGURE 3. (Color online) The same as in Fig. 2 for the PDF of the velocity components U_1 and U_3 of the harmonically bound BP, in the case of under damped dynamics.

were stored. The time series was used to estimate the corresponding nonequilibrium PDFs and correlation functions. It should be stressed that from these time series we eliminated the first 4×10^4 data in order avoid introducing into the calculations values corresponding to the first stages of the application of the harmonic force. The nonequilibrium velocity PDF, $W(U_1, U_3)$, obtained in numerical experiments for the case $\dot{\gamma} = 0.1$, is compared in Figs. 2 and 3 with their analytical counterparts as expressed by Eq. (27). Figure 2 corresponds to the critically-damped case, while Fig. 3 corresponds to under damped dynamics. First, it can be noticed that the analytical and numerical distributions are very similar and that a very good agreement between these two independent approaches is obtained. These figures illustrate that the effect of the imposed shear on $W(U_1, U_3)$ consists in spreading it over the direction of flow, as predicted in Sec. 2.

4.2. Velocity Correlation Functions

We also carried out the measurement of the two-time correlation functions $\langle\langle U_i(t') U_j(t) \rangle\rangle$, analytically derived through Eqs. (28)-(33) in Sec. 2.3.

Numerically, we calculated the correlations by using the time series of values of the velocity vector \vec{U} recorded during the experimental stage. In order to reduce the computational time used in the calculation of these functions, the complete series for each experiment was divided in 60 shorter series of equal length, extending over a period of 50 times the characteristic relaxation time $(\beta/2)^{-1}$. The correlation functions

were estimated for each one of these shorter series according to the usual formula

$$\langle\langle U_i(t + \tau) U_j(t) \rangle\rangle \simeq \frac{1}{\mathcal{N}_\tau} \sum_{\nu=1}^{\mathcal{N}_\tau} U_i(t_\nu + \tau) U_j(t_\nu), \quad (43)$$

where the index ν runs over the recorded values of the cut time series, and \mathcal{N}_τ is the total data available to perform the average corresponding to a time difference τ . Finally, the correlations obtained for all the short time series were averaged to give the final numerical estimation of $\langle\langle U_i(t') U_j(t) \rangle\rangle$. We applied this procedure to the ten time series corresponding to the five different values of the simulated velocity gradients and to the two restoring coefficients.

With the purpose of simplifying the subsequent comparison between the numerical and analytical results, we will introduce the notation Y_{ij} for correlations normalized with respect to their maximum value at equilibrium. In the analytical case the normalized functions are simply given by $Y_{ij} = M \langle\langle U_i(t + \tau) U_j(t) \rangle\rangle / k_B T$, while in the numerical case the normalization is performed by dividing with respect to the maximum value obtained experimentally for the correlation $\langle\langle U_1(t + \tau) U_1(t) \rangle\rangle$. We will also introduce the notation Y_{ij}^{eq} and Y_{ij}^{neq} , to represent, respectively, the equilibrium and nonequilibrium contributions of the normalized correlations, with $Y_{ij} = Y_{ij}^{\text{eq}} + Y_{ij}^{\text{neq}}$. Times t' and t will be also normalized with respect to the relaxation time $(\beta/2)^{-1}$, and we will introduce the symbol $\bar{\tau}$ to represent the dimensionless time difference $\bar{\tau} = \tau \beta/2 = (t' - t) \beta/2$.

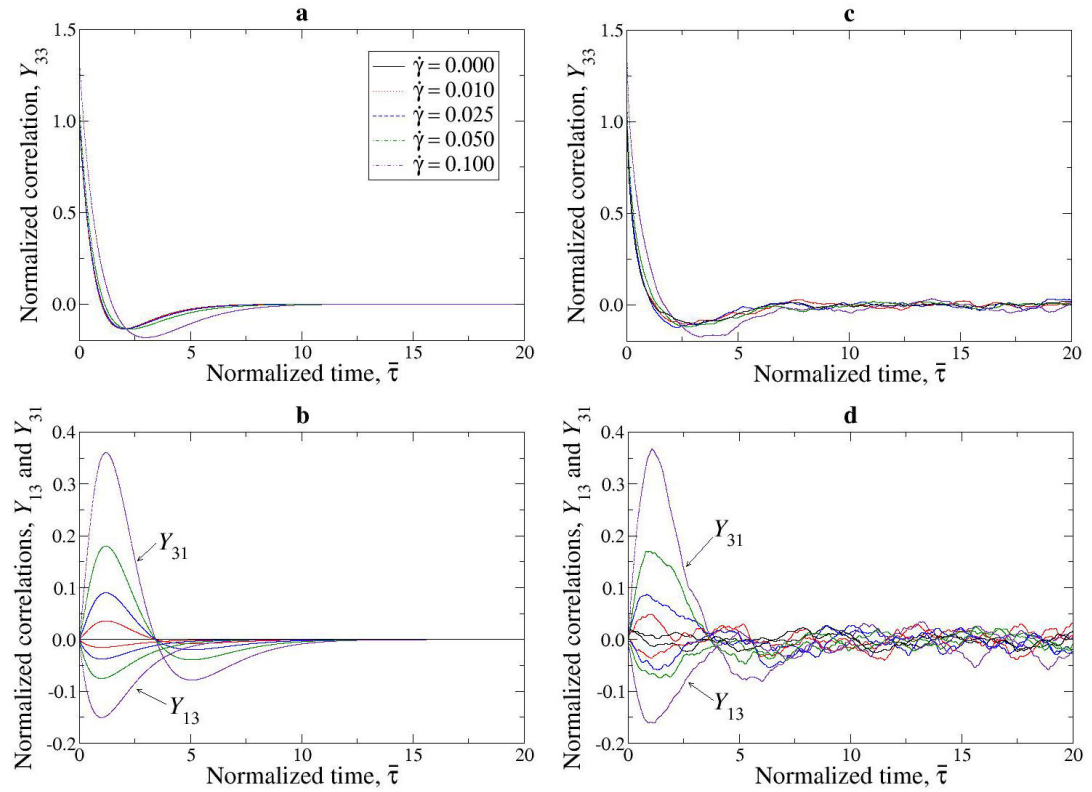


FIGURE 4. (Color online) Normalized correlations Y_{13} , Y_{31} and Y_{33} as function of the normalized time difference, $\bar{\tau}$, for a BP confined in a harmonic trap in sheared flows with different velocity gradients, $\dot{\gamma}$. Curves in cases **a** and **b** have been obtained from Eqs. (28)-(33); while curves in cases **c** and **d**, were calculated from independent numerical experiments based on MD and MPC. The specific simulation parameters correspond to a harmonic Brownian oscillator in the critically-damped case.

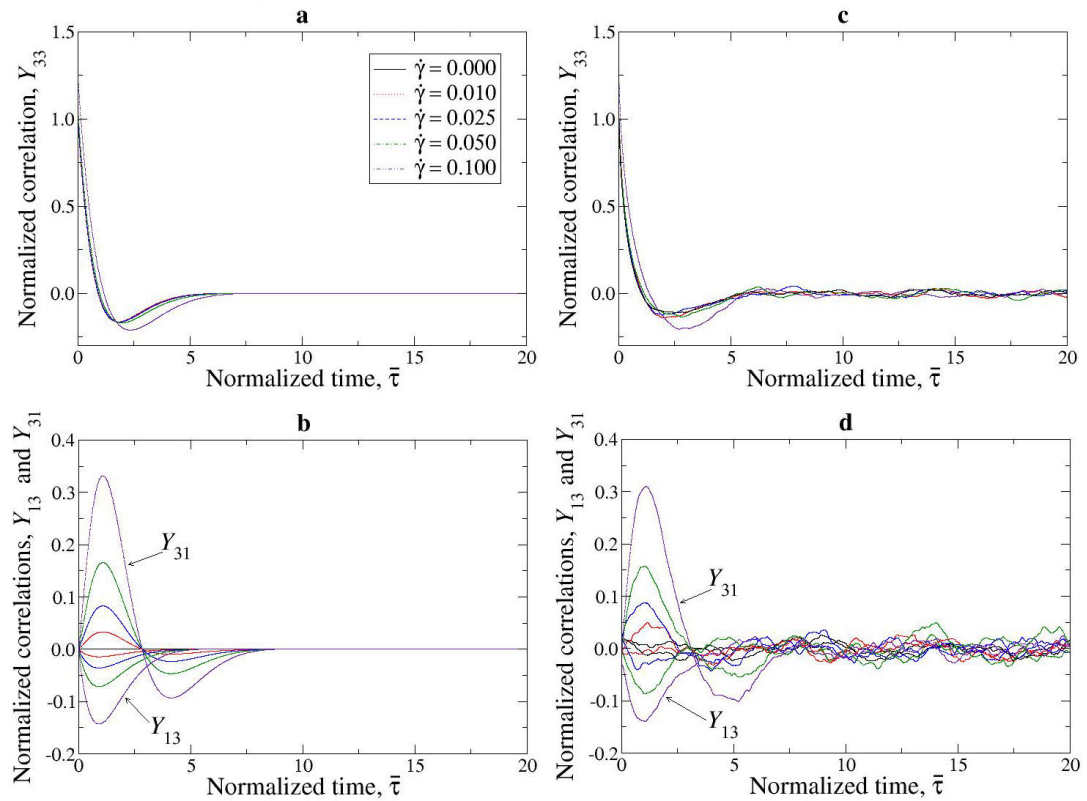


FIGURE 5. (Color online) The same as in Fig. 4 for a BP confined in a harmonic trap in the under damped regime.

We performed then the calculation of the correlation functions $Y_{13}(\bar{\tau})$, $Y_{31}(\bar{\tau})$ and $Y_{33}(\bar{\tau})$ in the nonequilibrium situations. We illustrate our results for the case of critically-damped harmonic Brownian motion in Fig. 4, and of under damped harmonic Brownian motion in Fig. 5, where the experimental and analytical correlation functions are directly compared. It can be observed once again that there is a very good agreement between these two independent approaches, and that correlations obtained from simulations exhibit precisely the behavior expected from the model based on Langevin dynamics. Specifically, the height of Y_{33} is observed to increase as function of $\dot{\gamma}$, while the cross-correlation functions Y_{13} and Y_{31} vanish in the equilibrium case and emerge with a clearly different time dependence when $\dot{\gamma} \neq 0$.

Curves presented in Figs. 4 and 5 show that the effects of the external shear on the correlation functions of the harmonically trapped BP can be significant even for small deviations from equilibrium. More precisely, it can be observed in those figures that a numerical velocity gradient with magnitude $\dot{\gamma} = 0.1$, corresponding to a Stokes number $\mathcal{S} = 0.4$, produces a nonequilibrium contribution Y_{33}^{neq} which has a magnitude about 30% of the equilibrium term Y_{33}^{eq} . In addition, for the same value of the Stokes number, $Y_{13}(\bar{\tau})$ reaches a maximum height whose magnitude represents about 16% of the maximum value of the equilibrium correlation Y_{33}^{eq} , while for the cross-correlation $Y_{31}(\bar{\tau})$ this percentage is about 35%.

These observations and those presented in Sec. 4.1 confirm the existence of the nonequilibrium effects induced by the coupling of the Brownian dynamics with the sheared bath. We conclude that the Langevin model from which these effects were derived is satisfactory within the range of the numerical parameters used in the present work.

It must be finally stressed that although the very good correspondence exhibited by the analytical and numerical curves in Figs. 4 and 5, a small difference between them can be observed consisting in that the numerical correlations extend in time over slightly longer periods than the theoretical correlations. The reason for this difference is that in the simulation method used in the present study, hydrodynamic correlations and compressibility effects are naturally incorporated via the application of the MPC algorithm [25, 26]. These effects are well known to produce a broadening of the correlation functions in the form of long-time tails [50–53], and can not be correctly obtained from the Langevin model presented here. An extension of the present analysis is under current research [36], in which compressibility and hydrodynamic effects on the dynamics of the harmonically bound BP in a shear flow are considered.

5. Conclusions

We have studied the Brownian motion of a particle confined in a harmonic trap and a nonequilibrium environment subjected to a uniform shear. For this purpose we have considered a Langevin model supplemented with the Faxén theorem

for describing the drag force on the particle and with the assumption that the stochastic forces have the same statistical properties than those observed in a bath in thermodynamic equilibrium, *i.e.* that stochastic forces follow a Markov-Gaussian process characterized by the classical Fluctuation-Dissipation relation. Based on this model, we have derived a formal expression for the PDF for observing the BP around a given point in its associated phase-space. This PDF turned out to be a Gaussian but, contrary to the case of harmonic Brownian motion in a fluid at rest, it exhibits anisotropic contributions increasing with the magnitude of the externally imposed shear. We have studied this effect in detail in the stationary limit, and shown that it could be significant even for small values of the Stokes number characterizing the deviations from equilibrium.

We have also used the Langevin model to calculate the effects that the external shear produces on the time-dependent correlation functions of the velocity of the confined BP. We have shown that the nonequilibrium bath causes an increment of the autocorrelation function along the direction of the external flow. Moreover, the imposed nonequilibrium state couples the components of the BP's velocity along the directions of the external shear and of the external velocity gradient. This coupling was found to increase linearly with the strength of the velocity gradient and to be non symmetric and time-irreversible.

In the second part of this work we have used a numerical method based on MD and MPC to simulate the motion of the harmonically confined BP in plane Couette flows with velocity gradients of diverse magnitude. This allowed us to measure from numerical experiments the nonequilibrium PDFs and correlation functions derived independently from the Langevin model. The numerical results were found to show the behavior predicted by the model, thus suggesting that this is good enough to describe the stochastic dynamics of the harmonically bound BP within the range of the selected simulation parameters. More importantly, the numerical results confirm the existence of the nonequilibrium coupling mechanism which breaks the spatial symmetry and time-reversibility of its dynamics.

The slight quantitative differences found between the analytical and the numerical results could be attributed to the incompleteness of the theoretical description, which is unable to describe the effects of compressibility and hydrodynamic correlations on the motion of the BP, while those are naturally incorporated by the used simulation technique.

It must be also stressed that our basic assumption concerning the independence of the stochastic forces on the external imposed shear, is not strictly correct [3, 22], and it could be interesting to consider the solution of the present problem from an alternative method, *e.g.* Mesoscopic Nonequilibrium Thermodynamics which would allow us to obtain a Fokker-Planck equation with corrections to the diffusion tensor, and to check whether they improve the agreement with the present numerical results.

Acknowledgments

H. Híjar thanks Universidad La Salle for financial support under grant I-062/12.

1. J. Keizer, *Statistical Thermodynamics of Nonequilibrium Processes* (Springer, New York, 1987).
2. S. R. de Groot and P. Mazur, *Non-Equilibrium Thermodynamics* (Dover, New York, 1984).
3. I. Santamaría-Holek, R. Lugo-Frías, R. F. Rodríguez and A. Gadomski, in *Thermodynamics-Physical Chemistry of Aqueous Systems*, edited by J. C. Moreno Piraján (InTech, 2011).
4. M. C. Marchetti and J. W. Dufty, *J. Stat. Phys.* **32** (1983) 255.
5. R. F. Rodríguez, E. Salinas-Rodríguez and J. W. Dufty, *J. Stat. Phys.* **32** (1983) 279.
6. G. Subramanian and J. F. Brady, *Physica A* **334** (2004) 343.
7. Y. Drossinos and M. W. Reeks, *Phys. Rev. E* **71** (2005) 031113.
8. J. M. Rubí and P. Mazur, *Physica A* **250** (1994) 253.
9. J. M. Rubí and A. Pérez-Madrid, *Physica A* **264** (1999) 492.
10. I. Santamaría-Holek, D. Reguera and J. M. Rubí, *Phys. Rev. E* **61** (2001) 051106.
11. D. Reguera, J. M. Rubí and J. M. G. Vilar, *J. Chem. Phys. B* **109** (2005) 21502.
12. I. Santamaría-Holek, J. M. Rubí and A. Pérez-Madrid, *New J. Phys.* **7** (2005) 35.
13. V. Breedveld, D. van den Ende, A. Tripathi and A. Acrivos *J. Fluid Mech.* **375** (1998) 297.
14. D. J. Pine, J. P. Gollub, J. F. Brady and A. M. Leshansky, *Nature* **438** (2005) 997.
15. J. S. Guasto, A. S. Ross and J. P. Gollub, *Phys. Rev. E* **81** (2007) 061401.
16. H. Orihara and Y. Takikawa, *Phys. Rev. E* **84** (2011) 061120.
17. S. Sarman, D. J. Evans and A. Baranyai, *Phys. Rev. A* **46** (1992) 893.
18. N. T. N. Phung, J. F. Brady and G. Bossis, *J. Fluid Mech.* **313** (1996) 181.
19. D. R. Foss and J. F. Brady, *J. Fluid Mech.* **407** (2000) 167.
20. C. Van den Broeck, J. M. Sancho and M. San Miguel, *Physica A* **116** (1982) 448.
21. A. Ziehl, J. Bammert, L. Holzer, C. Wagner and W. Zimmermann *Phys. Rev. Lett.* **103** (2009) 230602.
22. L. Holzer, J. Bammert, R. Rzehak and W. Zimmermann *Phys. Rev. E* **81** (2010) 041124.
23. H. Híjar, *J. Chem. Phys.* **139** (2013) 234903.
24. D. Frenkel and B. Smith, *Understanding Molecular Simulations: from Algorithms to Applications* (Academic Press, San Diego, 2002).
25. A. Malevanets and R. Kapral, *J. Chem. Phys.* **110** (1999) 8605.
26. A. Malevanets and R. Kapral, *J. Chem. Phys.* **112** (2000) 7260.
27. R. Kapral, *Adv. Chem. Phys.* **140** (2008) 89.
28. J. T. Padding and A. A. Louis, *Phys. Rev. E* **74** (2006) 031402.
29. M. Belushkin, R. G. Winkler and G. Foffi, *J. Phys. Chem. B* **115** (2011) 14263.
30. A. Nikobashman, C. N. Likos and G. Kahl, *Soft Matter* **9** (2013) 2603.
31. H. Faxén, *Arkiv för matematik, astr. och fysik Bd* **18** (1924).
32. P. Mazur and D. Bedeaux, *Physica* **76** (1974) 235.
33. S. Chandrasekhar, *Rev. Mod. Phys.* **15** (1943) 1.
34. R. F. Fox, *Phys. Rep.* **48** (1978) 180.
35. J. K. G. Dhont, *An introduction to dynamics of Colloids* (Elsevier, Amsterdam, 2003).
36. H. Híjar, (2014) in progress.
37. J. P. Hansen and I. R. McDonald, *Theory of simple liquids*, 2nd edition (Academic Press, London, 1986).
38. G. Gompper, T. Ihle, D.M. Kroll and R.G. Winkler, *Adv. Polym. Sci.* **221** (2009) 1.
39. J. M. Yeomans, *Physica A* **369** (2006) 159.
40. T. Ihle and D. M. Kroll, *Phys. Rev. E* **63** (2001) 020201.
41. T. Ihle and D. M. Kroll, *Phys. Rev. E* **67** (2003) 066706.
42. A. W. Lees and S. F. Edwards, *J. Phys. C* **5** (1972) 1921.
43. N. Kikuchi, C. M. Pooley, J. F. Ryder and J. M. Yeomans, *J. Chem. Phys.* **119** (2003) 6388.
44. E. Allahyarov and G. Gompper, *Phys. Rev. E* **66** (2002) 036702.
45. M. Hecht, J. Harting, T. Ihle and H. J. Hermann, *Phys. Rev. E* **72** (2005) 011408.
46. H. Híjar and G. Sutmann, *Phys. Rev. E* **83** (2011) 046708.
47. C. C. Huang, G. Gompper and R. G. Winkler, *Phys. Rev. E* **86** (2012) 056711.
48. C. M. Pooley and J. M. Yeomans, *J. Phys. Chem. B* **109** (2005) 6505.
49. E. Tüzel, M. Strauss, T. Ihle and D. M. Kroll, *Phys. Rev. E* **68** (2003) 036701.
50. B. J. Alder and T. E. Wainwright, *Phys. Rev. Lett.* **18** (1967) 988.
51. B. J. Alder and T. E. Wainwright, *Phys. Rev. A* **1** (1970) 18.
52. R. Zwanzig and M. Bixon *J. Fluid. Mech.* **69** (1975) 21.
53. H. J. H. Clercx and P. P. J. M. Schram, *Phys. Rev. A* **46** (1992) 1942.